Hindawi
Advances in Meteorology
Volume 2024, Article ID 4421766, 13 pages
https://doi.org/10.1155/2024/4421766

Research Article

Identifying the Moisture Sources in Different Seasons for Abaya-Chamo Basin of Southern Ethiopia Using Lagrangian Particle Dispersion Model

Israel Gebresilasie Kimo,[1] **Bisrat Elias Cholo**,[1] **and Tarun Kumar Lohani**[2]

[1]*Faculty of Meteorology and Hydrology, AWTI, Arba Minch University, P.O. Box 21, Arba Minch, Ethiopia*
[2]*Faculty of Hydraulic and Water Resources Engineering, AWTI, Arba Minch University, P.O. Box 21, Arba Minch, Ethiopia*

Correspondence should be addressed to Israel Gebresilasie Kimo; israel30907@gmail.com

Received 20 September 2023; Revised 20 December 2023; Accepted 29 December 2023; Published 9 January 2024

Academic Editor: Anzhen Qin

Understanding the sources of precipitation and their impacts is crucial for basin-wide water balance research. Previous research concentrated on the sources of moisture in Ethiopia. The southern part's moisture sources, however, were not investigated. The primary objective of this study is to trace the source of atmospheric moisture in the Abaya-Chamo sub-basin of southern Ethiopia using numerical water vapor tracers like Hybrid Single Particle Lagrangian Integrated Trajectory (HYSPLIT) model. Exploring the possible regions of atmospheric vapor roots and the path of moist air initiating rainfall that reaches the basin was feasible for the year 2018–2020. The anticyclone from the Arabian High, which is positioned in the Arabian and Mediterranean seas, was the primary source of moisture supply in the study area during the Belg (March to May) season, according to the back trajectory cluster analysis results. Additionally, the Indian Ocean adds moisture resulting from Mascarene highs brought by equatorial easterlies. Furthermore, during Kiremt (June to September), air masses from the Congo basin were the potential moisture source region for the study areas in combination with air masses originating from the Mascarene highs, located in the South Indian Ocean, and the St. Helena high, centered in the subtropical southern Atlantic Ocean. This study primarily focuses on the complex dynamics of atmospheric moisture sources around Abaya-Chamo sub-basin of southern Ethiopia, offering insight into seasonal fluctuations and contributing various components. These findings contribute to basin-specific water balance research by filling gaps in the previous studies.

1. Introduction

The scientific community has shown significant interest in identifying dominant moisture sources, employing various methods such as analytical models, isotopes, numerical atmospheric water tracers, and model sensitivity experiments [1]. HYSPLIT model with Graphical User Interfaces and a $1 \times 1^{\circ}$ climatic dataset derived from the Global Data Assimilation System has been utilized. This input is sourced from the National Oceanic and Atmospheric Administration (NOAA) Air Resources Laboratory's (ARL) archive to determine moisture sources and transport pathways. The Hybrid Single Particle Lagrangian Integrated Trajectory (HYSPLIT) model, a numerical water vapor tracer trajectory-based approach [2], is employed to detect the sources of moisture available for precipitation. This model has been widely used to assess global and regional sources in previous research [3–6].

The objective of this study is to trace the source of atmospheric moisture in the Abaya-Chamo sub-basin of southern Ethiopia using numerical water vapor tracers (HYSPLIT model).

The Abaya-Chamo sub-basin, situated in the southern part of Ethiopia within the Rift Valley basin, exhibits a warm semiarid tropical climate. Annual precipitation ranges from 665 mm to 1240 mm, with average temperatures varying between 8.8°C and 31.2°C [7].

In the southern part of Ethiopia, there is a bimodal rainfall pattern marked by extended periods of precipitation. The initial rainy season, known as Belg, occurs from March to May, while the second major rainy season occurs from mid-September to late November. However, from June to September, known as Kiremt, the area experiences minimal rainfall. Despite this, the regions consistently receive substantial rainfall during the specified intervals, playing a crucial role in shaping the distinctive climatic features of southern and south-eastern Ethiopia [8–10]. Despite previous studies in Ethiopia on atmospheric water vapor transport routes [11, 12], and vapor pathway detection using the Lagrangian model [13], there is a gap in understanding the moisture source for the Abaya-Chamo sub-basin, which has been taken into account.

Understanding precipitation sources and their contributions is vital for basin-wide water balance studies [6], hydrometeorological studies [5], land and water management practices [14], improving climate model parameterization and precipitation forecast accuracy [15], and for hydrology and meteorology, nurturing the importance of the global hydrological cycle in weather systems and water supplies [1].

The paper is organized as follows: Section 2 describes the model, data, and methods, with a particular emphasis on the datasets used in this study and the meteorological model preprocessing for identifying moisture sources and pathways, as well as ways to improve the quality of the trajectory (frequency analysis and trajectory analysis). Section 3 includes the findings and discussion, and Section 4 provides a summary of the findings.

1.1. Description of the Study Area

1.1.1. Location. Abaya-Chamo sub-basin is a component of the rift valley basin found in the southern portion of Ethiopia (Figure 1). The altitude of the region varies between 3478 m above mean sea level (a.m.s.l) (Mount Guge) and 1094 ma.m.s.l (at the outflow from the Chamo Lake). The area lies between 37°-38° east longitude and 5°–8° north latitude. Abaya-Chamo sub-basin includes the southern division of the key Ethiopian rift and neighboring highlands, largely placed in the SNNPR. The basin covers a surface area of about 18,600 km^2.

1.1.2. Climate. Abaya-Chamo basin is mostly characterized by a warm semiarid tropical climate, with yearly rainfall ranging from 665 mm to 1240 mm and average temperatures varying between 8.8°C and 31.2°C [7]. The climate is more characterized by a typical bimodal rainfall pattern with peaks from the end of March to mid of June (Belg season) and from mid of September to the end of November (Figure 2). Abaya-Chamo basin also has a high rate of evaporation (about 2300 mm per year in an average) and led by hot temperature all over the year. The great elevated area of the basin accepts advanced rainfall as related to the lesser elevated areas situated in the rift floor [8–10].

1.1.3. Hydrology. Gelana, Bilate, Gidabo, Hare, Baso, and Amessa are the main rivers that flow into Lake Abaya. Abaya Lake is also fed by a variety of minor brooks and ephemeral rivers. Sile, Argoba, Wezeka, and Sego are the rivers that join into Lake Chamo, as well as the overflow from Lake Abaya, which confluences with Kulfo River and finally drain to Lake Chamo. As a result of the hydrological interconnection between the two lakes, this basin is classified as a single basin [16].

For Bilate, Gelana, Gidabo, and Hare, the rivers in the Abaya-Chamo basin provide 383, 119, 189, and 60 mega cubic meters of water to Abaya Lake, respectively. Due to large flow of clayey to sandy clay soils transported from the surrounding mountains, the turbidity is high with brownish color. The level differences between the Abaya and Chamo lakes are 62 meters, Abaya Lake higher than Chamo Lake. The two lakes have been used for transportation, fishing, and tourism purposes. The lakes have not been sufficiently used intensively for irrigation [7].

2. Materials and Methods

2.1. Data Analysis. The meteorological daily precipitation data were gathered from the Ethiopian National Meteorology Institute for stations Abaya-Chamo basin from 1989 to 2019 and these climatological precipitation data have also been used to describe the climatology of the study area, and meteorological data for trajectory analysis is collected from NOAA ARL for the year 2018–2020.

2.2. Methods Used. The HYSPLIT Lagrangian multidimensional air mass velocity method, which has been utilized for atmospheric trajectory assessment for three years (2018–2020), was used to examine the possible areas of atmospheric water origin and the path of moist air leading to rainfall prior to arriving at Abaya-Chamo basin.

This study was carried out with the use of Tcl/Tk GUIs and the PC Windows-based HYSPLIT (Hybrid Single Particle Lagrangian Integrated Trajectory) model Version 5 produced by NOAA (National Oceanic and Atmospheric Administration). The model is based on the Lagrangian approach, which uses a changing frame of reference for determining advection and diffusion as air parcels travel away from their initial source, and the Eulerian methodology that employs a fixed three-dimensional grid as a frame of [2].

2.2.1. Meteorological Model Preprocessing. HYSPLIT utilizes a wide range of meteorological model data, from mesoscale to global scales, in its calculations. These meteorological data are already prepared for HYSPLIT, and the model was run through a trajectory simulation. The data include wind speed and direction, temperature, humidity, and rainfall. The majority of the data used by HYSPLIT are gridded outcomes of meteorological models, including several models executed at NOAA.

The HYSPLIT model was fed one degree by a one-degree climate data set produced by the global data assimilation system [2], https://www.ready.noaa.gov/HYSPLIT.php. These archives were accessed directly by using any FTP client. For this study, FileZilla Client has been used.

To compute a trajectory using the HYSPLIT model, specific inputs are essential, including the initial point, coordinates, elevation, and meteorological data files sourced

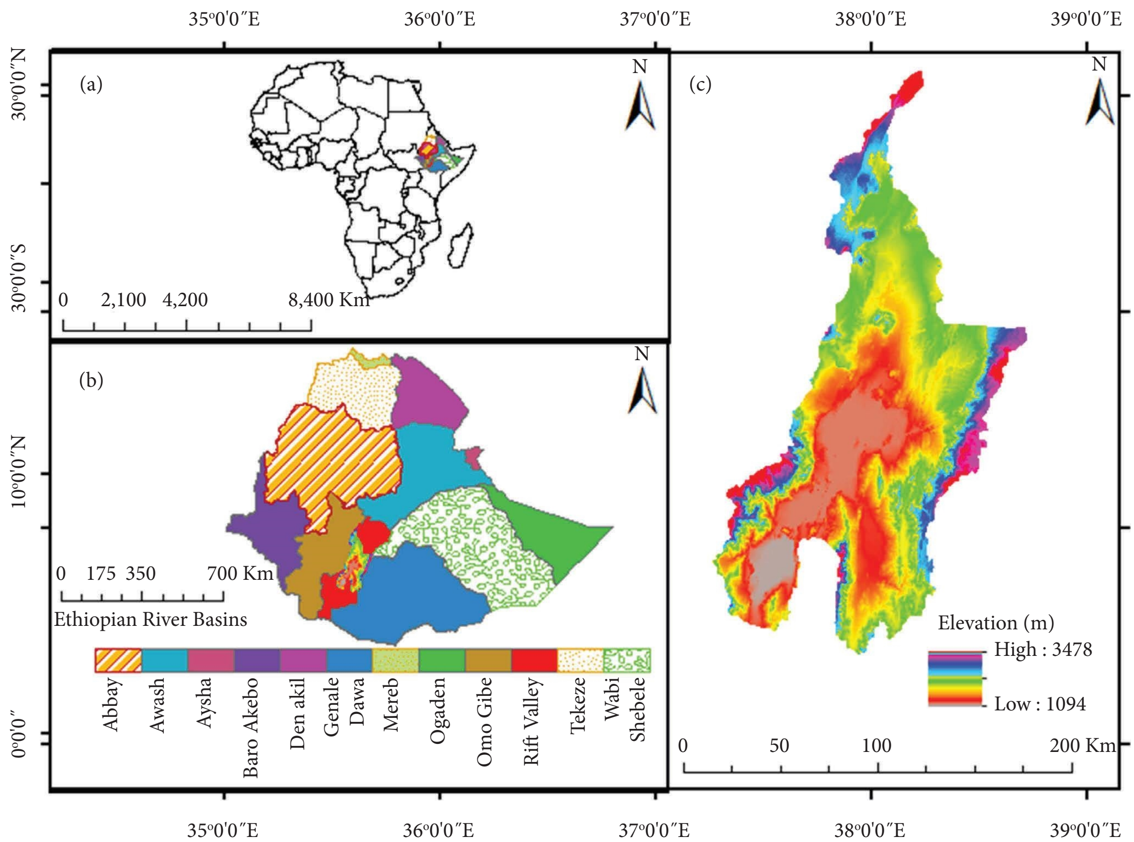

Figure 1: Location of the study area: (a) map of Africa, (b) Ethiopian river basin, and (c) Abaya-Chamo sub-basin.

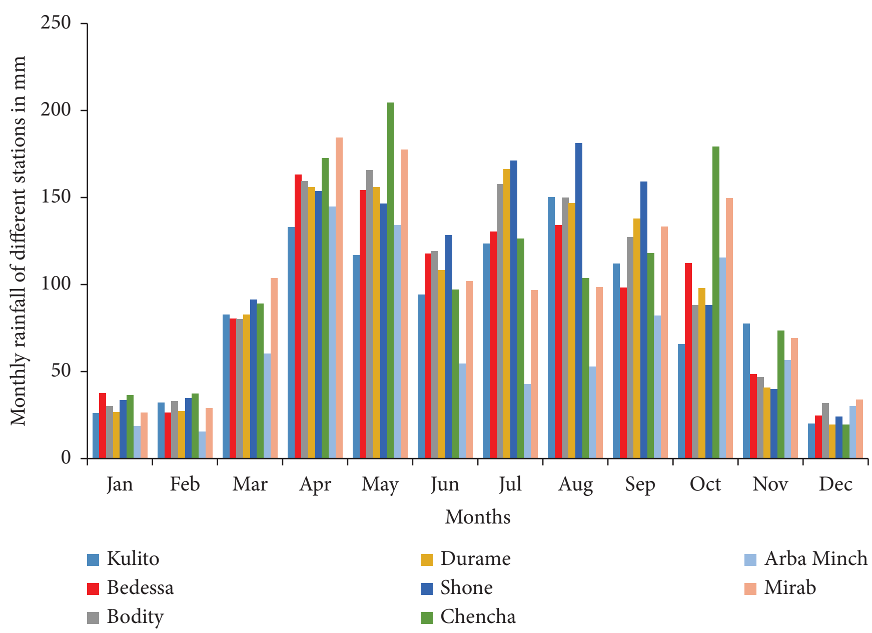

Figure 2: Monthly circulation of rainfall in mm from different meteorological stations in Abaya-Chamo basin (1989–2019).

from NOAA. The geographical location of Abaya-Chamo basin is 6.0141° N, 37.54588° E, and elevations of 1000, 1500, and 2000 meters were utilized in the model. Additionally, the model requires total run times, with a duration of 10 days (240 hours) selected in this case, aligning with the average period of atmospheric water presence [17]. The HYSPLIT algorithm, along with the GDAS dataset, has been extensively documented [2, 18].

2.2.2. Frequency Analysis. One of the methods of analyzing several trajectory output files is to use frequency analysis. In this analytical methodology, multiple trajectories were consolidated into a single output file, with each file containing a particular path generated from a distinct run of the trajectory model. In this study, frequency analysis has been performed for the rainy seasons of Belg (March–May), Kiremt (June–mid-September), and other rainy periods (September–November).

The two processes are accomplished by execute display of frequency analysis. The first step is to count how many trajectories are included in every grid cell that spans the whole region of the grid resolution set at one degree by default. Different resolutions are selectable from the menu. The ratio of the amount of trajectories (T) that traveled through each (i, j) grid cell and the total number (N) of trajectories studied results in the trajectory frequency (F) as follows:

$$Fi, j = 100 \sum Ti, \ \frac{j}{N}. \tag{1}$$

If the residence time radio button is not set to Yes, each trajectory in the source location grid cell is counted only once, and each trajectory is counted once for each intersecting grid cell as follows:

$$\sum Ti, j \leq 1. \tag{2}$$

In the latter segment of execute display, the display for the output of trajectory frequency is triggered to open automatically. This display shows the flow in all directions throughout the season.

2.2.3. Cluster Analysis. To further analyze the paths and validate the reliability of the trajectory analysis, a huge set of trajectories incoming at the research location was subjected to cluster analysis, grouping analogous trajectories together. This analysis was conducted for both the source locations and all similar trajectories.

This method involves combining close trajectories and representing such groupings, referred to as clusters, by their average trajectories. In a cluster, the disparities between trajectories are reduced, whereas disparities among clusters are emphasized. Trajectories are joined computationally until the overall change of the separate routes around their group average begins to rise. This happens after two or more clusters are merged.

Using the cluster analysis tool included in the HYSPLIT model, many homogenous air mass trajectories were combined into clusters, and the mean of each cluster was utilized to display the dominating trajectory patterns in this study.

2.2.4. Clustering Equations. The spatial variance (SV) between each endpoint (k) along the trajectory (j) inside its cluster (i) is estimated during the clustering process as follows:

$$\mathrm{SV}i, j = \sum k\,(pj, k - Mi, k)\hat{}2. \tag{3}$$

The sum over the amount of destination along the trajectory is calculated, where P and M represent the position vectors for the individual trajectory and its cluster average trajectory, correspondingly. The cluster spatial variance (CSV) is obtained by summing the spatial variances of all trajectories within the cluster as follows:

$$\mathrm{CSV}i = \sum j\mathrm{SV}i, j. \tag{4}$$

The sum of the CSV for all clusters adds up to provide the total spatial variance (TSV) as follows:

$$\mathrm{TSV} = \sum i\mathrm{CSV}j, k. \tag{5}$$

Clustering begins with each trajectory being assigned to a specific cluster, in order that here are i clusters per $j = 1$ trajectory in every cluster. The amount of cluster stay decreased in one iteration when two clusters joined. In order that after the second repetition, there will be i-1 groups, with one cluster comprising of two paths and the remaining clusters each having one trajectory. This procedure persists until there is only a solitary cluster remaining.

During every repetition, the total sum of variances (TSV) is calculated for each possible combination of merging clusters. This involves adding the trajectories from Cluster 1 to those in Cluster 2, Cluster 3, and so on until the TSV is computed for all remaining combinations of clusters. This results in (i^2-i)/2 computations per iteration. The combination with the lowest TSV is selected and carried forward to the next iteration. This process continues until there is only one cluster remaining. Enormous clusters of trajectories move comparatively slower to complete the clustering process. The TSV increases rapidly at first and then peaks for the remainder of the iterations until toward the end of the computation, when different clusters begin to combine and the TSV increases again.

The HYSPLIT model's calculations of a single backward trajectory are not exact but may have considerable ambiguity. The predicted horizontal ambiguity of the HYSPLIT trajectory estimation is 10–20% of the journey distance [16]. The accuracy of the trajectory analyses would be increased by performing a statistical analysis that involves examining a substantial number of trajectories incoming at Abaya-Chamo sub-basin [19].

To increase the validity of the air mass history and the dependability of the HYSPLIT-generated back trajectories, several quality control procedures were employed in this study [20].

To begin, the initial task involved computing the flight paths for three altitudes: 1000, 1500, and 2000 meters above the surface. These altitudes corresponded to barometric surfaces approximately at 900, 850, and 800 hPa. At these pressure levels, the resolution errors are negligible, suggesting that these errors are negligible, increasing the accuracy level of the results. Second, the percentage of a grid cell that a path is acceptable to transport in one advection time step, TRATIO (0.25), was employed in this investigation. The trajectory calculation inaccuracy of the HYSPLIT model is decreased by smaller TRATIO values. Third, numerical examination of a large number of trajectories incoming at the research location was used to confirm the accuracy of the trajectory analysis (trajectory cluster analysis). In order to aggregate trajectories with similar paths, the HYSPLIT model does a trajectory group analysis.

These flight paths that were computed close to one another are combined in the cluster analysis and those clusters are represented by their mean trajectory; when the disparities between clusters increases, the differences between paths within a cluster decrease. Trajectories are joined computationally to reduce the number of clusters until the entire spatial variance (TSV) begins to rise noticeably. This normally happens after different clusters are merged. This amount of clusters is then picked because the ideal cluster numbers are considered for selecting and mixing comparable trajectories. The general flowchart of the study is depicted in Figure 3.

3. Results and Discussion

3.1. Frequency Analysis

3.1.1. Belg Season. The result of frequency analysis execute display gives the information about two routes. The initial step is to tally how many trajectories fall within each grid cell that covers the region. At the grid resolution of 0.25° and the count of flight paths that fall within each grid cell, covering the respective areas, there are 288, 288, and 288 trajectories for the years 2018, 2019, and 2020 of March to May (Belg season), respectively. The next portion executes the display and opens the display of the trajectory frequency output, which indicates the flow in all directions during the season (Figure 4).

Trajectory is believed to pass through a grid square if there is at least one endpoint that falls within the grid square and the result also prevails that what percent of the trajectories pass through any given grid square. So, the blue color indicates more than 10% of the trajectories passing in a grid square and the green color represents the trajectory that pass more than 1% in a grid square.

3.1.2. Kiremt Season. The frequency analysis outcome at 0.25° grid resolution and the number of paths inside each grid cell that covers the area are 276, 276, and 276 trajectories for the Kiremt seasons of 2018, 2019, and 2020, respectively (Figures 5(a)–5(c)). If at least one endpoint of a trajectory lies within the grid rectangle, it is assumed that the trajectory passes through it.

The outcome also determines what percentage of path travels over every given grid box, with blue indicating more than 10% of trajectories passing via a grid box and green indicating more than 1% of trajectories that traverse a specific grid square.

3.2. Cluster Analysis

3.2.1. Mean Cluster Analysis for Belg Season. The distribution of vapor trajectories (cluster means) for rainfall times between March and May for the years 2018, 2019, and 2020 is presented in Figure 6. The numbers in brackets show the cluster numbers (1^{st}–5^{th}) including the percentages of all trajectories allocated to every of the five clusters. The outcome for the 2018 Belg season, as indicated in Figure 6(a), in the Arabian sea and Indian ocean contributes about 29% and 28%, respectively.

For 2019, Figure 6(b) reveals that the Indian Ocean and Arabian Sea contribute more about 37% and 35%, respectively, while the southern Indian Ocean and the Mediterranean Sea added less about 4% and 1% over the study area for the Belg season, respectively.

Figure 6(c) for 2020 represents the Arabian Sea contributing more than 33%, despite the fact that the southern Indian Ocean and Red Sea contribute less than about 9% and 6%, respectively, for Belg season over the study area. Due to the presence of overlapping branches and the repeated entry and exit of parcels in the target region, the cumulative numbers do not reach 100% as there is some discrepancy. Due to the presence of overlapping branches and the repeated entry and exit of parcels in the target region, the cumulative numbers do not reach 100% as there is some discrepancy.

The possible source of precipitation for the study area from March to May (Belg season) 2020 is shown in Figure 7; the lines represent the starting points of the calculated backward trajectories for 10 days. The star shows the study area's location. The results of each of the five clusters are given in the left and right columns.

The result prevails that the potential moisture source for the study areas during Belg season is anticyclone from the Arabian High, which is located in Arabian Sea, Mediterranean Sea, and the Indian Ocean owing to Mascarene Highs carried by the equatorial easterlies. This is because the Azores High, located in the northeast Atlantic, experiences a diminished intensity compared to its usual strength. Consequently, it yields to the southward movement of midlatitude storms, which traverse across the Mediterranean Sea and extend into the Middle East [21]. The circulation anomalies linked to these storms that propagate eastwards cause the Arabian High to shift in a southward direction, relocating it towards the northwestern Indian Ocean. This displacement of the Arabian High into the Indian Ocean results in an amplified transport of moisture towards Ethiopia, leading to an increase in rainfall during the Belg season [22].

Diro et al. [22] also confirmed that during the Belg rainy season, the significant weather patterns linked to variations in rainfall are characterized by the Arabian High abnormal humidity over eastern Africa, and deviations in low-level winds originating from the Indian Ocean [11, 12].

3.2.2. Mean Cluster Analysis for Kiremt Season. In the Kiremt season, Figure 8 depicts the circulation of air mass trajectories (cluster means) for rainfall days. The numbers in

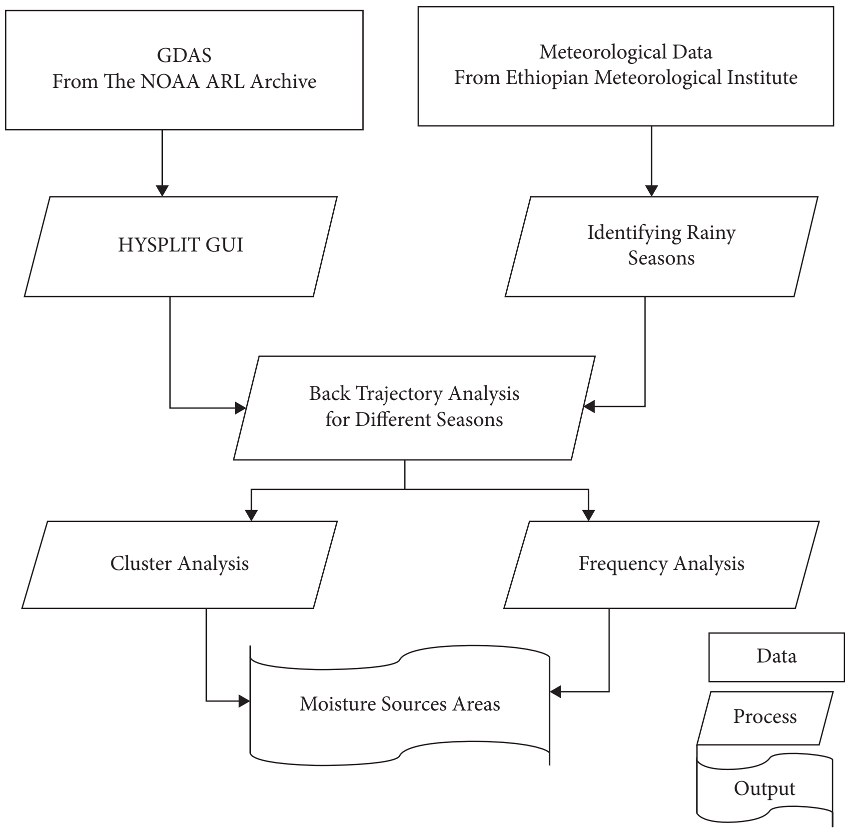

Figure 3: Flowchart to introduce the data process.

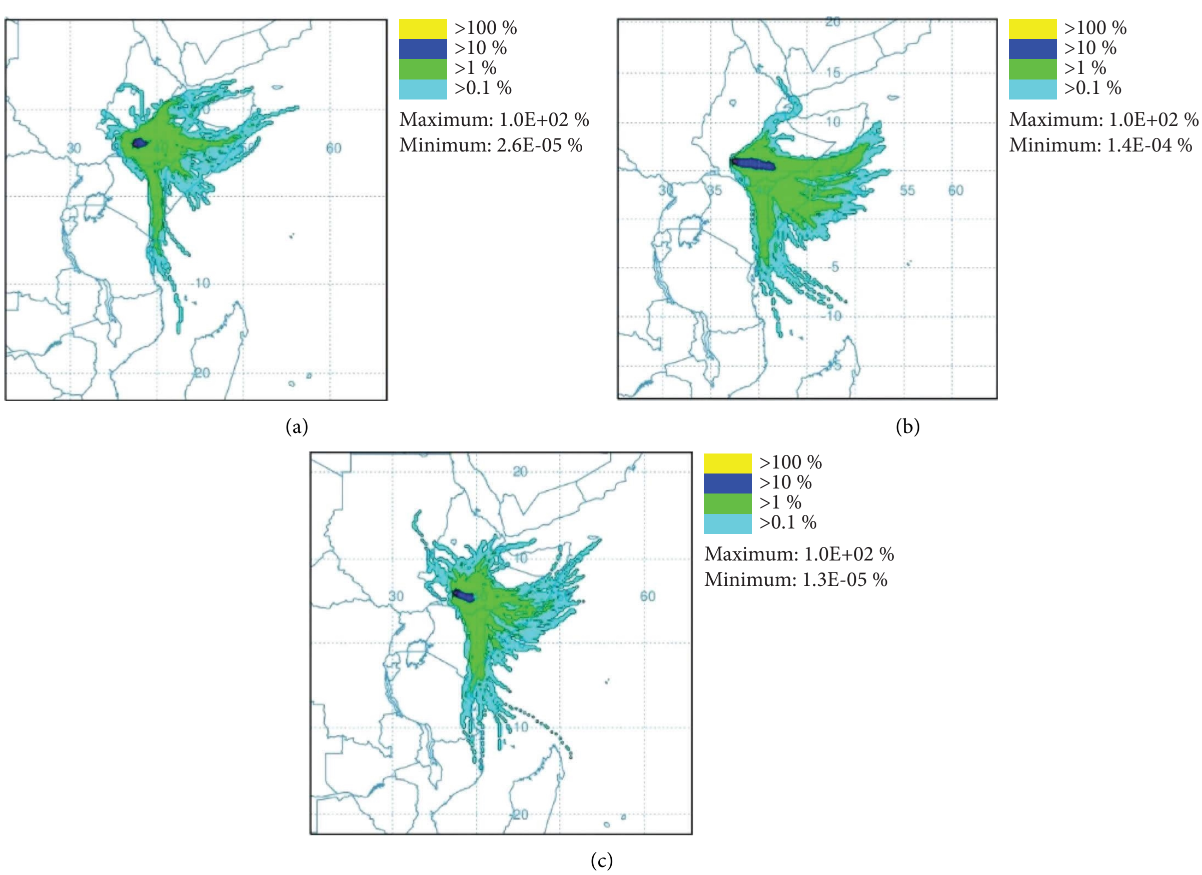

Figure 4: Trajectory frequency for Belg seasons: (a) 2018, (b) 2019, and (c) 2020.

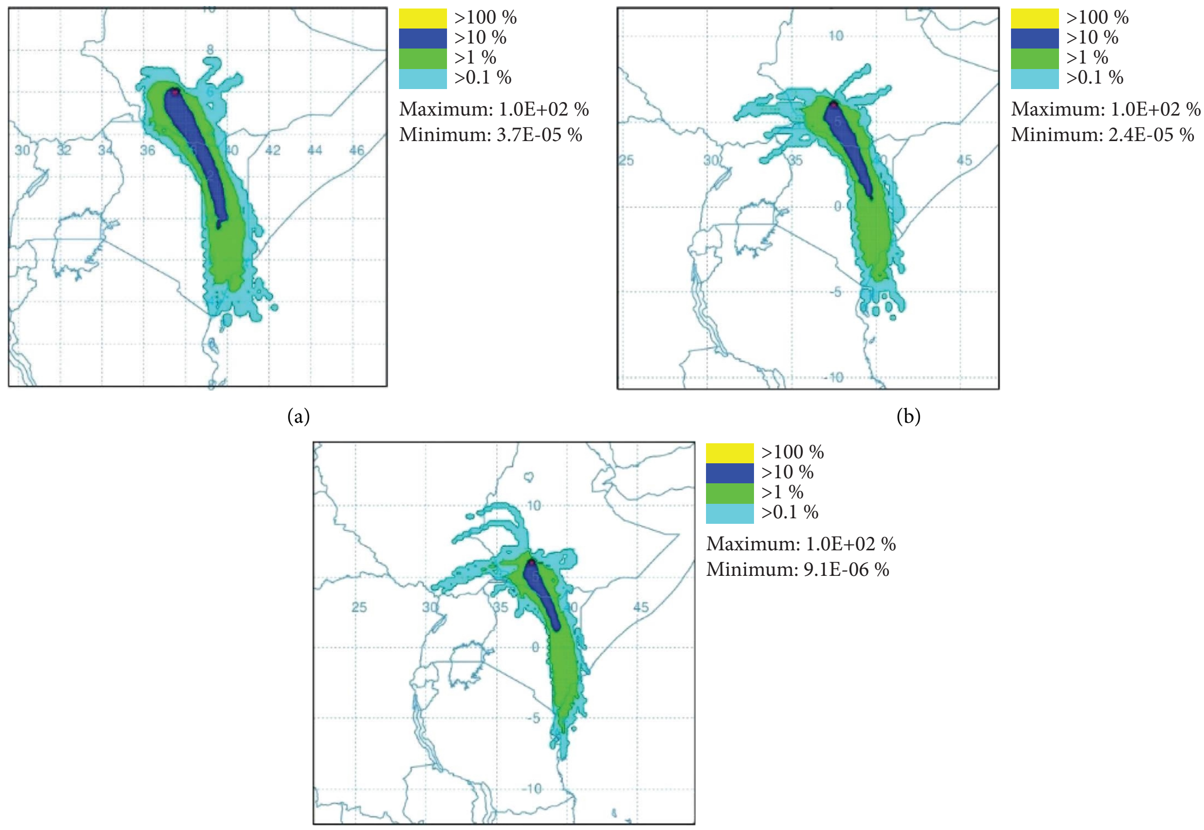

(c)

Figure 5: Trajectory frequency for Kiremt seasons: (a) 2018, (b) 2019, and (c) 2020.

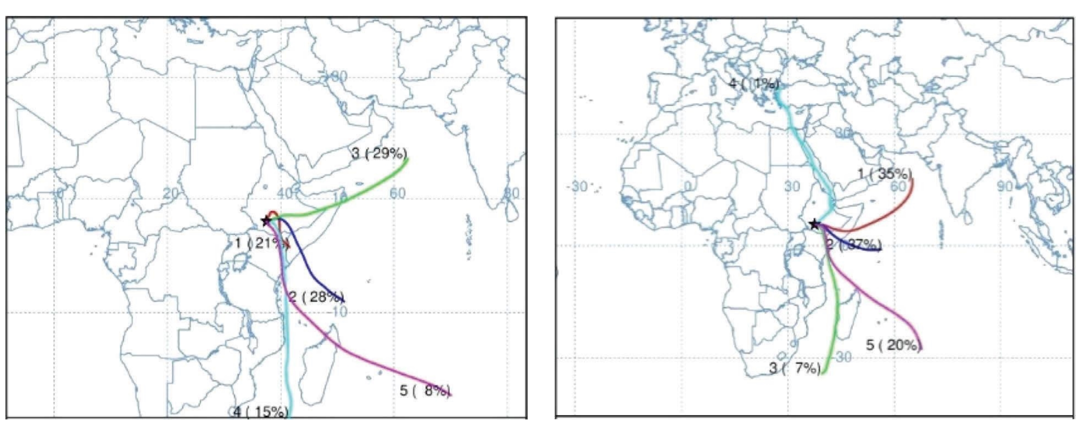

(a) (b)

Figure 6: Continued.

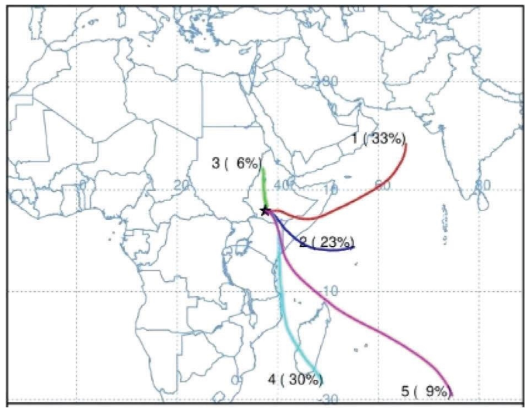

(c)

Figure 6: Mean cluster analysis for Belg seasons: (a) 2018, (b) 2019, and (c) 2020.

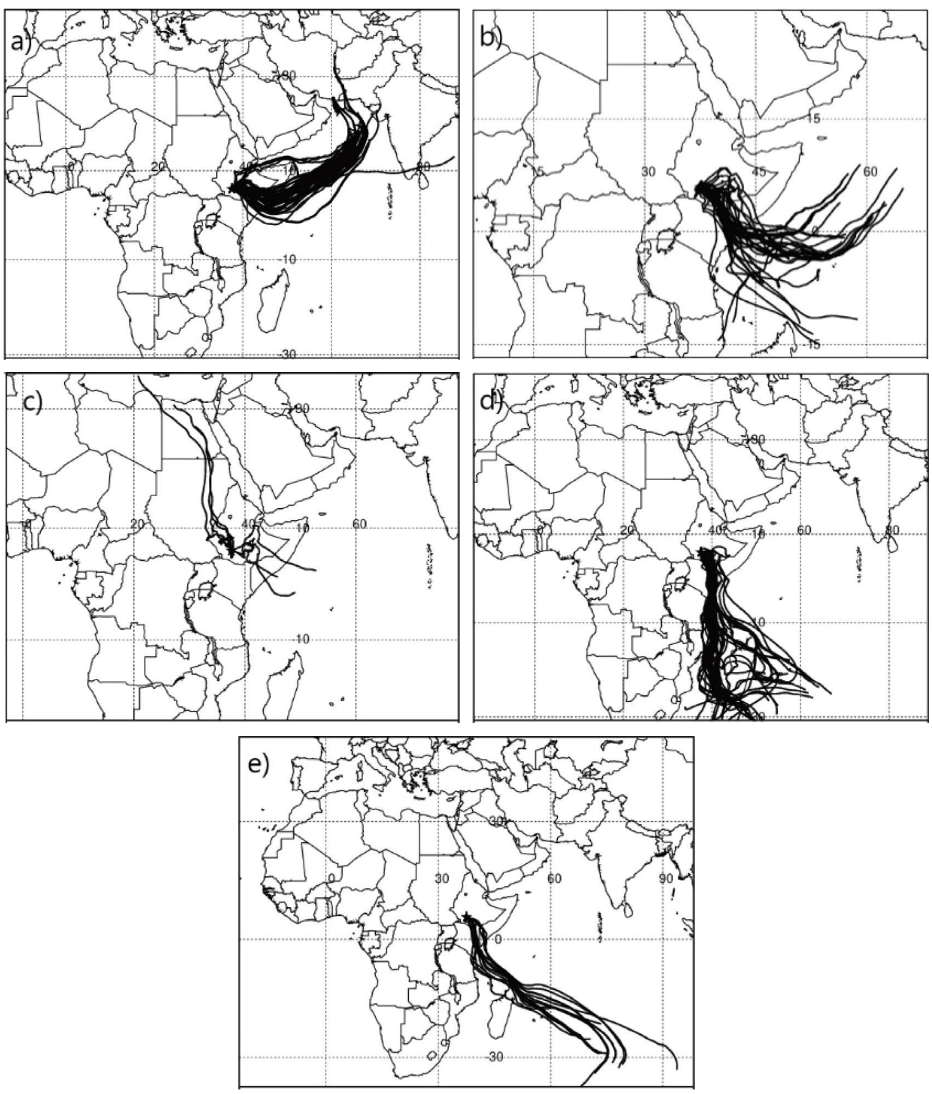

Figure 7: Potential source areas of precipitation in the study area in Belg season 2020: (a) 1st cluster, (b) 2nd cluster, (c) 3rd cluster, (d) 4th cluster, and (e) 5th cluster.

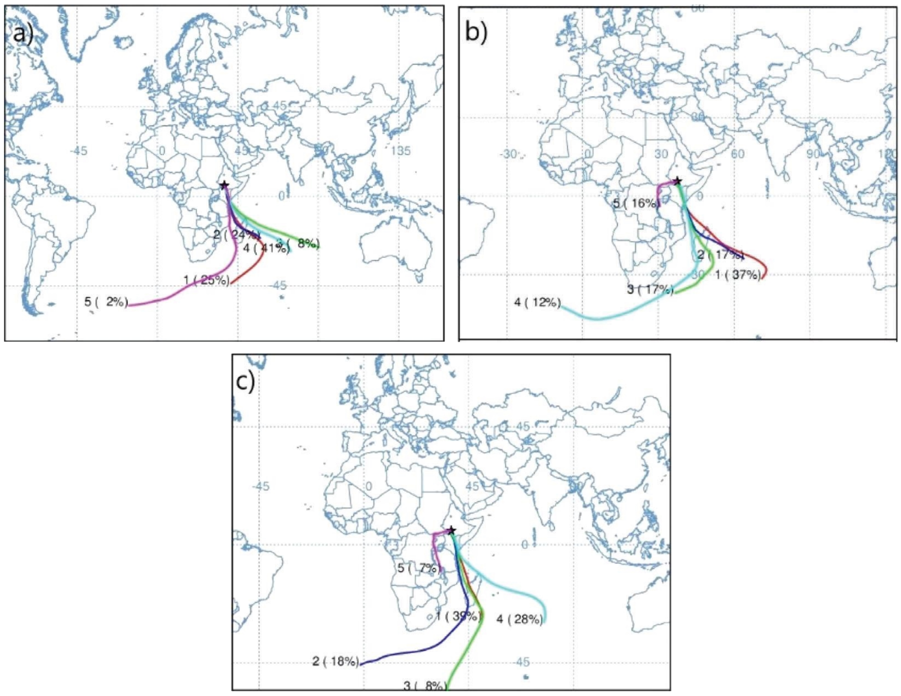

Figure 8: Vapor trajectories (cluster means) for Kiremt: (a) 2018, (b) 2019, and (c) 2020.

the brackets represent the number of clusters (1–5), and the numbers inside represent the proportion of all trajectories belonging to each of the five groupings. The result shows that for the year 2018 (Figure 8(a)), the South Indian Ocean (south-easterlies) contributes more than about 41% and South Atlantic Ocean (southwesterly) contributes less than 2% for Kiremt season over the study area. For the year 2019, Figure 8(b) reveals that the Indian Ocean and Congo basin contribute more than about 37% and 16%, respectively, whereas the South Atlantic Ocean added about 12% over the study area for the Kiremt season, respectively. Figure 8(c) for the year 2020 represents that the South Indian Ocean contributes more than about 39% and the South Atlantic Ocean and Congo basin contribute less about 18% and 7%, respectively, for Kiremt season over the study area.

Due to the presence of overlapping branches and the repeated entry and exit of parcels in the target region, the cumulative numbers do not reach 100% as there is some discrepancy. Figure 9 depicts the Kiremt season's possible precipitation source for Abaya-Chamo sub-basin. The lines represent the beginning places for 10 days calculating their previous movement or origin. The star on the map denotes the specific location of the study area. The outcomes of each of the five clusters are displayed in the left and right columns.

The potential moisture source regions for the study areas during Kiremt season are the Mascarene High which are found in South Indian Ocean and the anticyclone in the subtropical southern Atlantic Ocean (St. Helena high). Furthermore, the continental source like air masses that originated from Congo basin is responsible for the Kiremt season rainfall. This was attributed in part to the excessive specific humidity and in part to the enormous amount of air passing through these pathways. Despite the excessive specific humidity of the Gulf of Guinea low-level air current, the net moisture input from the Congo basin was considered substantially lower than that from the other regions. This is because just a small part of the air reaching Ethiopia comes from the Congo basin [13].

The enhancement of the gentle winds originating from the west over Central Africa and Western equatorial Africa could potentially result in a direct impact of the intensifying movement of air from the Gulf of Guinea towards Ethiopia. The link between stronger westerly over Africa's Central Region and increased Kiremt rainfall in Ethiopia might be attributed to direct or incidental factors such as deviations in convection, which are linked to the ITCZ position and strength [3, 21, 23–26]. The size and strength of the subtropical high-pressure systems known as the Mascarene and St Helena cells are commonly associated with the rainfall patterns in Ethiopia. When sea surface temperatures (SSTs) are low in these regions, it leads to the reinforcement of the St Helena and Mascarene highs, which, in turn, facilitates greater moisture transport towards Ethiopia.

Consequently, the rainfall in Ethiopia tends to be amplified when there is a strengthening of both the Mascarene and St. Helena subtropical high-pressure systems, along with the accompanying Mozambique ridge. The main outcome of this strengthening is an intensified south-to-north airflow across the equator, which promotes a more vigorous monsoon season over the Horn of Africa. Previously, wet summers in Ethiopia were linked in general, a reinforcement of the summer circulation pattern leads to a strengthening of various atmospheric phenomena. This strengthening involves intensified pressure gradients from north to south across Africa, heightened intensity of the Intertropical Convergence Zone (ITCZ), increased strength of low-level westerly winds,

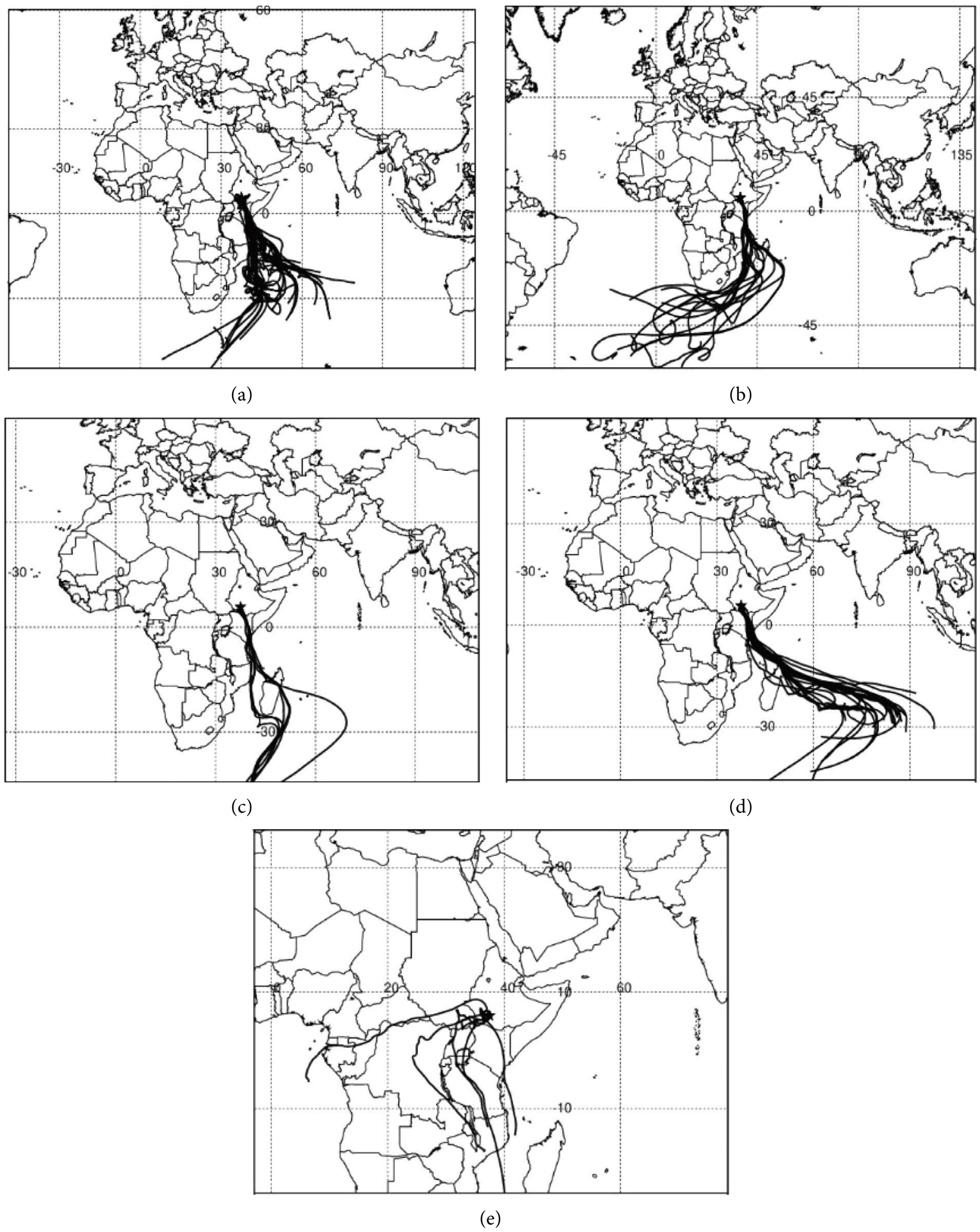

Figure 9: Potential source areas of precipitation in the study area in Kiremt season 2020: (a) 1st cluster, (b) 2nd cluster, (c) 3rd cluster, (d) 4th cluster, and (e) 5th cluster.

enhanced intensity of the Somali Jet, and an augmentation of the upper-level Tropical Easterly Jet. Conversely, a weakening of the summer circulation would have the opposite effect on these atmospheric features [21, 26].

3.3. HYSPLIT Model Result at Different Barometric Surfaces. The back-calculated trajectories in Figure 6 and the trajectory cluster analysis in Figure 8, both at barometric surfaces (850 hPa), along with a path at three other barometric surfaces (900, 850, and 800 hPa), illustrate that there is no distinction in the paths and origins of air masses across various atmospheric layers, suggesting a barotropic nature of the atmosphere. As a result, the selection of the pressure level for the HYSPLIT trajectories is unlikely to alter the outcomes, indicating consistency in the results.

As seen in the trajectory map (Figure 10), most of the air entering the Abaya-Chamo basin via the African lands to the south originates from the Indian Ocean. Although the prevailing direction of the air mass indicates that it originates from the southwest, implying an Atlantic source, it is important to note that there is a minor contribution to this airflow from the Congo basin as well.

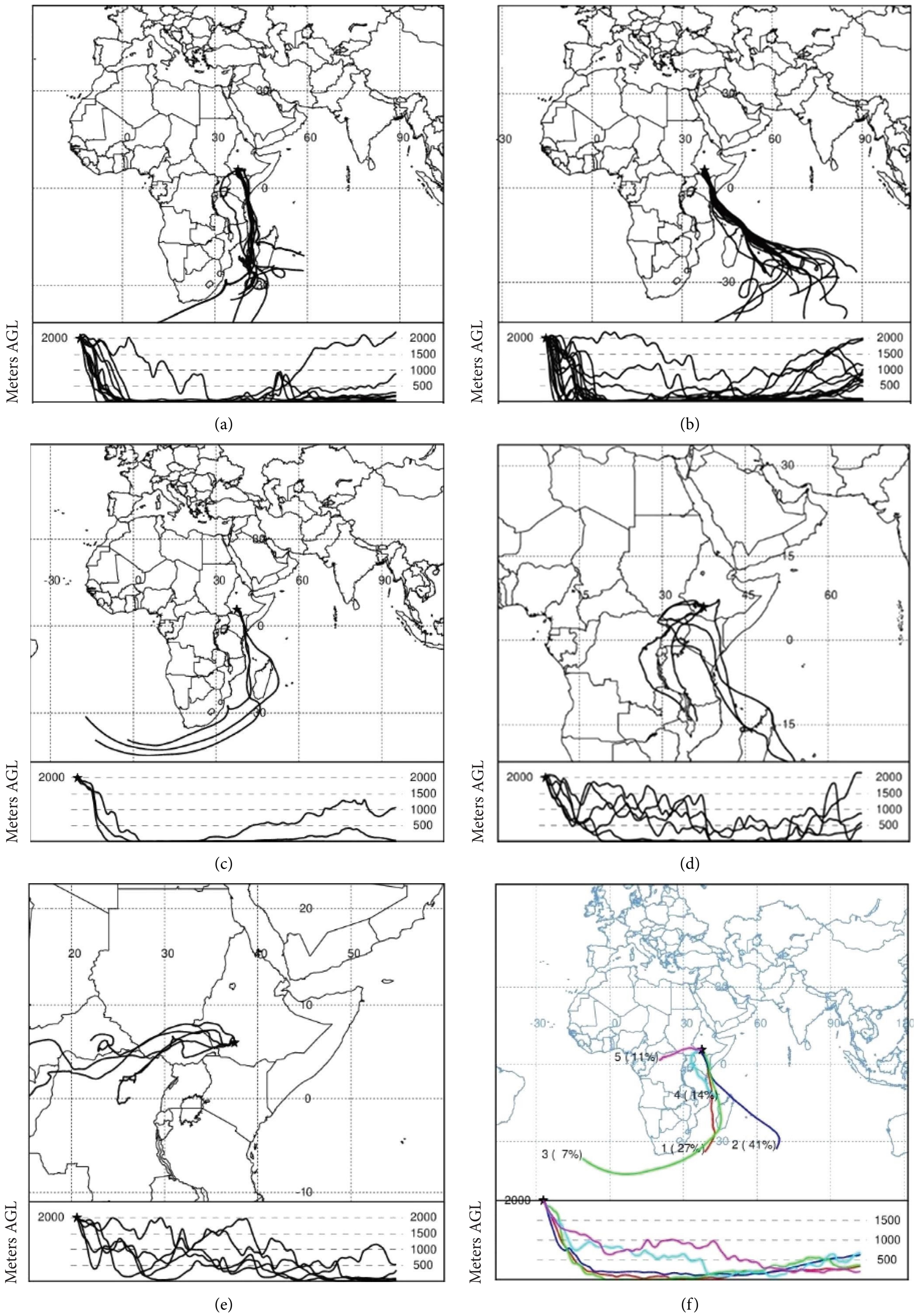

Figure 10: Trajectory cluster analysis at 800 hPa for Kiremt season: (a) 1st cluster, (b) 2nd cluster, (c) 3rd cluster, (d) 4th cluster, (e) 5th cluster, and (f) mean cluster.

Table 1: Summary of HYSPLIT model output for the year 2018–2020 indicating the possible moisture source regions respective to their percentage contribution at different seasons.

Year	March to May		June to August		September to November	
2018	Indian Ocean	68%	South Indian Ocean	96%	South Indian Ocean	87%
	Arabian Sea	31%	South Atlantic Ocean	2%	Arabian Sea	13%
	Mediterranean Sea	1%	Congo basin	2%		
2019	Indian Ocean	60%	South Indian Ocean	75%	South Indian Ocean	83%
	Arabian Sea	39%	Congo basin	12%	Arabian Sea	17%
	Mediterranean Sea	1%	South Atlantic Ocean	13%		
2020	Indian Ocean	59%	South Indian Ocean	62%	South Indian Ocean	87%
	Arabian Sea	33%	Congo basin	9%	Arabian Sea	12%
	Mediterranean Sea	9%	South Atlantic Ocean	29%		

The summarized findings in Table 1 imply that for the indicated years during March to May, Indian Ocean is the main origin of humidity, followed by Arabian Sea and Mediterranean Sea. Furthermore, during June to August, South Indian Ocean is the major moisture source region followed by South Atlantic Ocean and Congo basin. For the period of September to November, South Indian Ocean is the main moisture source region while Arabian Sea contributes less moisture for Abaya-Chamo basin [27].

4. Conclusion

The HYSPLIT model has provided valuable insight into the moisture sources that contribute to the Abaya-Chamo Basin during various rain seasons. The study has shown that the basin receives moisture from both oceanic and continental sources with different regions contributing during different seasons. During the Belg season (March to May), the Arabian high anticyclone located in the Arabian and Mediterranean Seas is a potential moisture source. The Indian Ocean, especially the Mascarene Highs carried by the equatorial easterlies, also contributes moisture during this season. The combination of these two sources results in the basin receiving substantial moisture. During the Kiremt season (June to September), Mascarene Highs located in the South Indian Ocean, St. Helena high centered in the subtropical southern Atlantic Ocean, and the Congo basin are the potential moisture sources for the Abaya-Chamo Basin. These multiple sources likely contribute to the variability in rainfall patterns observed during this season. Throughout the months from September to November, the South Indian Ocean and Arabian Sea are the potential moisture sources. These sources are anticipated to contribute to the basin's rainfall picks.

The findings of this study may be scientifically used for water resource management and agriculture in the Abaya-Chamo Basin. Understanding the sources of moisture that initiates the rainfall basin can help in providing valuable information for water allocation and crop management. As climate change continues to impact rainfall patterns in the region, this information will be crucial in developing adaptation strategies to ensure sustainable water and food security for the communities living in and around the basin.

Data Availability

The data used in this study are available from the corresponding author on special request.

Additional Points

List of Abbreviations. Abbreviations used in the text have been defined in the text at first use, and a list of abbreviations is provided wherever necessary.

Conflicts of Interest

The authors declare that they have no conflicts of interest.

Authors' Contributions

Israel Gebresilasie Kimo conceptualized the study and wrote and prepared the original draft. Bisrat Elias Cholo has prepared figures, graphs, and tables. Tarun Kumar Lohani visualized the study and revised and edited the manuscript. All authors have read the manuscript and agreed for publication.

Acknowledgments

The authors are thankful to Arba Minch University for receiving all logistics support in conducting this research work.

References

[1] L. Gimeno, A. Stohl, R. M. Trigo et al., "Oceanic and terrestrial sources of continental precipitation," *Reviews of Geophysics*, vol. 50, no. 4, 2012.

[2] A. F. Stein, R. R. Draxler, G. D. Rolph, B. J. Stunder, M. D. Cohen, and F. Ngan, "NOAA's HYSPLIT atmospheric transport and dispersion modeling system," *Bulletin of the American Meteorological Society*, vol. 96, no. 12, pp. 2059–2077, 2015.

[3] K. Soderberg, S. P. Good, M. O'Connor, L. Wang, K. Ryan, and K. K. Caylor, "Using atmospheric trajectories to model the isotopic composition of rainfall in central Kenya," *Ecosphere*, vol. 4, no. 3, pp. 1–18, 2013.

[4] S. Wang, M. Zhang, J. Crawford, C. E. Hughes, M. Du, and X. Liu, "The effect of moisture source and synoptic conditions on precipitation isotopes in arid central Asia," *Journal of Geophysical Research: Atmospheres*, vol. 122, no. 5, pp. 2667–2682, 2017.

[5] S. Jana, B. Rajagopalan, M. A. Alexander, and A. J. Ray, "Understanding the dominant sources and tracks of moisture for summer rainfall in the southwest United States," *Journal of Geophysical Research: Atmospheres*, vol. 123, no. 10, pp. 4850–4870, 2018.
[6] N. Le Duy, I. Heidbüchel, H. Meyer, B. Merz, and H. Apel, "What controls the stable isotope composition of precipitation in the Mekong Delta? A model-based statistical approach," *Hydrology and Earth System Sciences*, vol. 22, no. 2, pp. 1239–1262, 2018.
[7] A. Teklemariam and B. Wenclawiak, "Water quality monitoring within Abaya and Chamo drainage basin," *Lake Abaya Research Symposium Proceedings*, vol. 4, pp. 109–116, 2004.
[8] N. Wagesho, N. K. Goel, and M. K. Jain, "Temporal and spatial variability of annual and seasonal rainfall over Ethiopia," *Hydrological Sciences Journal*, vol. 58, no. 2, pp. 354–373, 2013.
[9] A. Gebremichael, S. Quraishi, and G. Mamo, "Analysis of seasonal rainfall variability for agricultural water resource management in southern region, Ethiopia," *Journal of Natural Sciences Research*, vol. 4, no. 11, pp. 56–79, 2014.
[10] A. WoldeYohannes, M. Cotter, G. Kelboro, and W. Dessalegn, "Land use and land cover changes and their effects on the landscape of Abaya-Chamo Basin, Southern Ethiopia," *Land*, vol. 7, no. 1, p. 2, 2018.
[11] N. E. Levin, E. J. Zipser, and T. E. Cerling, "Isotopic composition of waters from Ethiopia and Kenya: insights into moisture sources for eastern Africa," *Journal of Geophysical Research: Atmospheres*, vol. 114, 2009.
[12] S. Kebede and Y. Travi, "Origin of the δ18O and δ2H composition of meteoric waters in Ethiopia," *Quaternary International*, vol. 257, pp. 4–12, 2012.
[13] E. Viste and A. Sorteberg, "Moisture transport into the Ethiopian highlands," *International Journal of Climatology*, vol. 33, no. 1, pp. 249–263, 2013.
[14] R. J. Van der Ent, O. A. Tuinenburg, H. R. Knoche, H. Kunstmann, and H. H. Savenije, "Should we use a simple or complex model for moisture recycling and atmospheric moisture tracking?" *Hydrology and Earth System Sciences*, vol. 17, no. 12, pp. 4869–4884, 2013.
[15] J. Worden, D. Noone, and K. Bowman, "Importance of rain evaporation and continental convection in the tropical water cycle," *Nature*, vol. 445, no. 7127, pp. 528–532, 2007.
[16] S. B. Awulachew and H. H. Horlacher, "Development and application of 2-parameters monthly water balance model in limited data situation, the case of Abayachamo basin, Ethiopia," *Zede Journal*, vol. 17, pp. 56–69, 2000.
[17] J. R. Gat, "Atmospheric water balance—the isotopic perspective," *Hydrological Processes*, vol. 14, no. 8, pp. 1357–1369, 2000.
[18] S. Aryalakshmi and D. Madhu, "Moisture trajectories during heavy rainfall events using Hybrid Single-Particle Lagrangian Integrated Trajectory (HYSPLIT) model," *Journal of Physics: Conference Series*, vol. 2070, no. 1, Article ID 012066, 2021.
[19] M. Cabello, J. A. Orza, V. Galiano, and G. Ruiz, "Influence of meteorological input data on backtrajectory cluster analysis a seven-year study for southeastern Spain," *Advances in Science and Research*, vol. 2, no. 1, pp. 65–70, 2008.
[20] I. Pisso, E. Sollum, H. Grythe et al., "The Lagrangian particle dispersion model FLEXPART version 10.4," *Geoscientific Model Development*, vol. 12, no. 12, pp. 4955–4997, 2019.
[21] Z. T. Segele, P. J. Lamb, and L. M. Leslie, "Large-scale atmospheric circulation and global sea surface temperature associations with Horn of Africa June–September rainfall," *International Journal of Climatology*, vol. 29, no. 8, pp. 1075–1100, 2009.
[22] G. T. Diro, D. I. Grimes, and E. Black, "Teleconnections between Ethiopian summer rainfall and sea surface temperature: part II. Seasonal forecasting," *Climate Dynamics*, vol. 37, no. 1-2, pp. 121–131, 2011.
[23] T. Gissila, E. Black, D. I. Grimes, and J. M. Slingo, "Seasonal forecasting of the Ethiopian summer rains," *International Journal of Climatology*, vol. 24, no. 11, pp. 1345–1358, 2004.
[24] D. Korecha and A. G. Barnston, "Predictability of june–september rainfall in Ethiopia," *Monthly Weather Review*, vol. 135, no. 2, pp. 628–650, 2007.
[25] Y. Seleshi and U. Zanke, "Recent changes in rainfall and rainy days in Ethiopia," *International Journal of Climatology*, vol. 24, no. 8, pp. 973–983, 2004.
[26] C. J. Williams and D. R. Kniveton, *African Climate and Climate Change: Physical, Social and Political Perspectives*, Springer, Dordrecht, Netherlands, 2011.
[27] K. Costa, J. Russell, B. Konecky, and H. Lamb, "Isotopic reconstruction of the African humid period and Congo air boundary migration at Lake Tana, Ethiopia," *Quaternary Science Reviews*, vol. 83, pp. 58–67, 2014.